



Multi-objective optimization of cylindrical segmented tubes as energy absorbers under oblique crushes: D-optimal design and integration of MULTIMOORA with combinative weighting

Hamidreza Souzangarzadeh¹ · Ali Jahan² · Mohammad Javad Rezvani¹ · Abbas S. Milani³

Received: 7 March 2019 / Revised: 21 October 2019 / Accepted: 6 January 2020 / Published online: 5 March 2020
© Springer-Verlag GmbH Germany, part of Springer Nature 2020

Abstract

Vehicles experience off-axial loads as well as axial loads during collisions. Hence, it is essential to have oblique loads be involved in investigating thin-walled tubes in vehicles as energy absorbers. In this paper, to find the optimum design of a segmented tube in terms of various collision scenarios, the RSM D-Optimal Design is used along with MULTIMOORA as a multiple-attribute decision-making (MADM) method. The tube consists of three parts having different thicknesses and lengths. Energy absorption, initial peak load, and maximum load in three angles of loads (0° , 15° , and 30°), and masses of the tube were defined as independent objectives. Design points were constructed to obtain all responses through finite elements method (FEM). It was found that the obtained models of responses predict the crashworthiness with acceptable accuracy. Then the optimization provides fifteen Pareto front designs of tubes through fifteen different scenarios. Finally, the integration of MULTIMOORA within a combinative weighting method selected the best tube from the optimums. The contrast between the optimum basic tube and the selected segmented tube demonstrated that the latter was capable of increasing the energy absorption by 24–41%, and reducing the initial peak load by 50–60% for the three applied loads.

Keywords Energy absorber · MULTIMOORA · Combinative weighting method · D-optimal · Design of experiments (DOE)

1 Introduction

The application of energy absorbers, as thin-walled structures, has proliferated in transport industries, particularly the automobile industry (Lu and Yu 2003), since the possibility of dissipating crash energy and reducing the peak crush loads, caused by a severe collision, has made this kind of structures noticeably effective and practicable for safety purposes (Saeidi Gooagarchin et al. 2018). Thin-walled tubes have acceptable behavior under dynamic loadings, low-cost manufacturing, and availability. Thus, several experimental, theoretical, numerical, and optimal investigations have been conducted to study the various shapes of the tubes as energy absorbers under different conditions to enhance

their performance in crashworthiness terms (Zhang et al. 2018; Zahran et al. 2018; Ravi Sankar and Parameswaran 2018; Eyvazian et al. 2018; Taştan et al. 2016; Khalkhali et al. 2016; Niknejad et al. 2015; Song et al. 2013). To lessen the aggressiveness of crashes in low-speed collisions, segmented tubes were introduced and investigated in the literature (Jafarian and Rezvani 2019; Souzangarzadeh et al. 2017; Jandaghi Shahi and Marzbanrad 2012). These tubes often have several segments, with each having a specific thickness and length, creating load-displacement response with an overall positive slope during crushing.

Although all the above-mentioned studies concentrated on the energy absorbers, crashing behavior under pure axial loads, in practice, experiencing pure axial loads is uncommon in crashes like automobile crashes. In fact, they become deformed under oblique loads. The off-axial loads lead to more complicated crushing such as global bending collapsing mode and reduction in energy absorption. As stated by the automotive industry requirements, the bumper structures should be practicable under 30° angle loads (Reyes et al. 2003). Therefore, a number of studies have

Responsible Editor: Mehmet Polat Saka

✉ Hamidreza Souzangarzadeh
hamid.reza.sou@gmail.com

Extended author information available on the last page of the article.

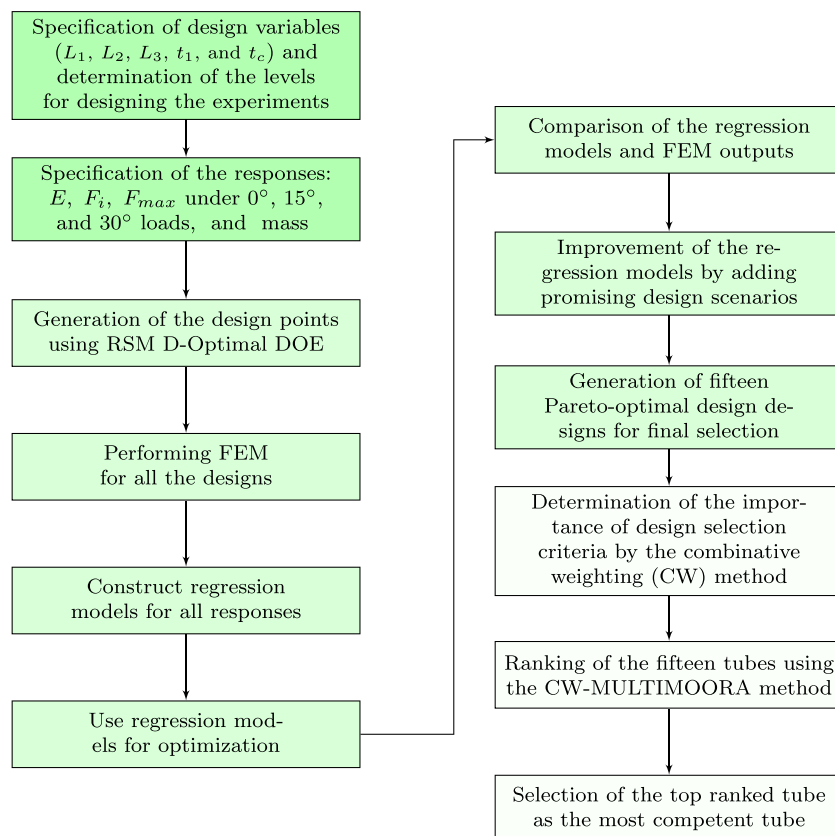
investigated the design and optimization of energy absorbers concerning oblique loading (Ying et al. 2017; Gao et al. 2016; Wang et al. 2016; Djamaluddin et al. 2018; Qi et al. 2012; Alavi Nia et al. 2012). Alkhatib et al. (2018) studied corrugated tapered tubes under seven different loading angles. Tran and Baroutaji (Tran and Baroutaji 2018) determined the optimal design of multi-cell triangular tubes under multiple loading angles. In the majority of thin-walled tubes under axial loading, the maximum crushing load (F_{max}) occurs at the first stage of collapsing; therefore, it is equal to the initial peak load (F_i) (Chen et al. 2018; Zhang et al. 2018). However, in some tubes, specially under oblique loads, the maximum load is not the initial peak load (Ghamarian and Zarei 2012; Tasdemirci et al. 2015; Zhang and Zhang 2016; Kathiresan and Manisekar 2016; Song et al. 2013). Song et al. (2013) optimized a foam-filled conical tube based on the initial peak load, maximum peak load, mean load, and SEA (specific energy absorption). In virtue of time and cost of experimental trails and numerous design points required for the optimization problems, many researchers have used numerical simulation to optimize design of energy absorbers such as straight tubes under oblique loads (Ying et al. 2017; Gao et al. 2016; Sun et al. 2018; Djamaluddin et al. 2015; Yang and Qi 2013), tapered tubes under oblique loads (Zhang et al. 2014; Qi et al. 2012),

and tubes under axial loadings (Song et al. 2013; Khalkhali et al. 2016; Baykasoğlu and Baykasoğlu 2017).

Although energy absorbers offer many advantages, the decidedly high initial peak load is one of their vital deficiencies, which might cause fatalities or serious harm to the passengers during the crash. Reducing the peak loads, particularly the initial one, is desirable in minimizing the impact loads transmitted to the vehicle. Therefore, to narrow the transmitted initial peak load, various approaches have been presented such as working on designs inspired by the coconut tree (Ha et al. 2018), presenting crochet-sintered mesh tube (CSMT) for composite tubes (Wu et al. 2018), and using hybrid reinforced composite (Supian et al. 2018).

To achieve an optimal vehicle structure in terms of crashworthiness, researchers must commonly consider several different objectives that must be minimized and/or maximized at the same time. In the majority parts of the literature on energy absorbers, maximum crush load, and SEA have served as two primary objectives optimization (Pirmohammad et al. 2019; Qi et al. 2012; Gao et al. 2016; Djamaluddin et al. 2015). Many researchers have employed the design of experiments in the optimization process of energy absorbers (Ying et al. 2017; Firouzi et al. 2018; Zhang et al. 2014). Yang and Qi (Yang and Qi 2013) employed D-optimal in addition to an optimization

Fig. 1 Flowchart of the proposed method for optimization and selection of cylindrical segmented tubes under oblique loading scenarios



algorithm to investigate empty and foam-filled square columns under oblique loading. Djameluddin et al. (2015) optimized foam-filled double cylindrical tubes under axial and oblique loads by NSGA II and D-optimal. Decision-making methods are the competent means of selecting the most favorable alternative based on all design decision-maker’s evaluation criteria (Jahan et al. 2016). In the manufacturing process of loudspeakers, Maghsoodia et al. (2018) used and proposed a novel multi-criteria decision-making (MCDM) approach to select the optimal prototype design. Čereška et al. (2018) evaluated various metal screw joints by four selection methods (SAW, TOPSIS, COPRAS, and EDAS). The Full Multiplicative Form of Multiple Objective Optimization on the basis of Ratio Analysis (MULTIMOORA) method, as a robust multi-objective decision-making technique (Hafezalkotob et al. 2018), has been effectively employed in diverse fields of studies (Brauers et al. 2013; Deliktas and Ustun 2017; Adalı and Işık 2017; Zhao et al. 2016; Fattahi and Khalilzadeh 2018; Zavadskas et al. 2015; Stanujkic et al. 2015; Hafezalkotob et al. 2016a; Liu et al. 2019; Ijadi Maghsoodi et al. 2018; Zavadskas et al. 2017; Abdi 2018; Ding and Zhong 2018).

The present study first presents a description of the cylindrical segmented tube design problem, including the geometrical parameters and responses of the structure under oblique loadings. Then, the optimization of the structure by means of D-optimal is realized and the most efficient design is selected through a combination of an extended MULTIMOORA (Hafezalkotob and Hafezalkotob 2016) and a combinative weighting (CW) (Jahan et al. 2012) method.

2 Materials and methods

Figure 1 presents the proposed procedure for finding and selecting the most efficient design of the cylindrical segmented tube for crashworthiness applications.

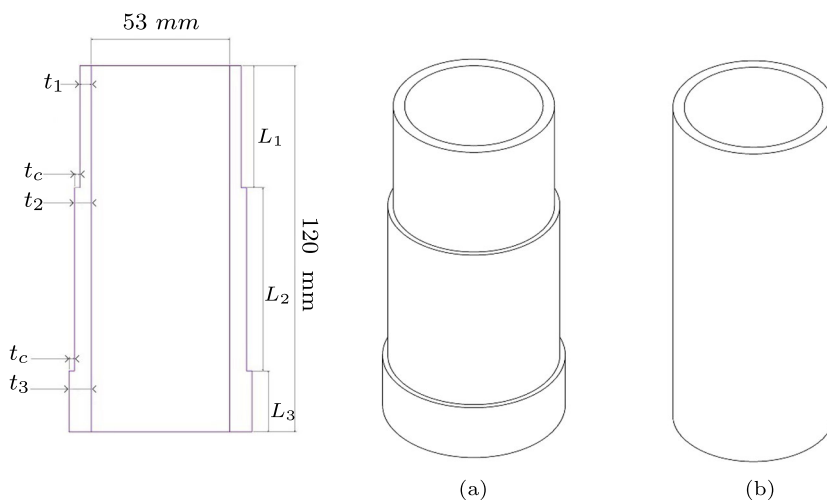
2.1 Geometry of design problem and the application of the D-optimal method

According to the proposed procedure in Fig. 1, the D-optimal design of experiments (DOE) and the finite element method (FEM) are to be used to construct the regression models. They specifically relate crushing characteristics to geometrical parameters of the structure. The segmented steel tubes were simulated using FEM under crush loads. The segmented tubes consist of three sections with different lengths and thicknesses (Fig. 2). The thickness of the second and third sections (t_2 and t_3) was enlarged by t_c to be thicker than the preceding ones, which means

$$\begin{cases} t_2 = t_1 + t_c \\ t_3 = t_2 + t_c \end{cases} \quad (1)$$

The whole length, L_{total} , and the diameter, D , were considered to be 120 mm and 53 mm, respectively. The length of sections (L_1 , L_2 , and L_3), the thickness of the first section (t_1), and thickness factor (t_c) were employed as independent structural parameters of all design points; L_{total} remained fixed, and the range of t_1 was selected based on the former designs (Jafarian and Rezvani 2019; Souzangarzadeh et al. 2017; Jandaghi

Fig. 2 Independent variables used in the design of **a** the cylindrical segmented tube and **b** basic tube



Variables	-1	0	+1
Length of sections (L_1 , L_2 , and L_3)	20	40	60
Thickness of first section (t_1)	1	1.4	1.8
Thickness factor (t_c)	0.3	0.5	0.8

Table 1 The dimensions of the D-optimum design points used in the study

Design points	L_1 mm	L_2 mm	L_3 mm	t_1 mm	t_c	Design points	L_1 mm	L_2 mm	L_3 mm	t_1 mm	t_c
1	60	40	20	1	0.3	18	40	20	60	1.4	0.8
2	40	60	20	1	0.3	19	40	60	20	1.8	0.3
3	60	20	40	1	0.3	20	20	60	40	1.8	0.3
4	20	60	40	1	0.3	21	40	20	60	1.8	0.3
5	40	20	60	1	0.3	22	60	20	40	1.8	0.3
6	20	40	60	1	0.3	23	40	40	40	1.8	0.3
7	20	60	40	1	0.5	24	20	40	60	1.8	0.3
8	60	40	20	1	0.5	25	60	40	20	1.8	0.3
9	40	20	60	1	0.8	26	20	60	40	1.8	0.8
10	20	60	40	1	0.8	27	60	20	40	1.8	0.8
11	40	60	20	1	0.8	28	20	40	60	1.8	0.8
12	60	40	20	1	0.8	29	40	20	60	1.8	0.8
13	60	20	40	1	0.8	30	60	40	20	1.8	0.8
14	20	60	40	1.4	0.3	31	40	60	20	1.8	0.8
15	60	20	40	1.8	0.5	32	20	40	60	1	0.8
16	40	40	40	1	0.8	33	40	20	60	1.4	0.5
17	40	40	40	1.4	0.5	34	40	60	20	1.4	0.3

Shahi and Marzbanrad 2012). To operate DOE, thirty-four design points, as different combinations of the values of independent variables, were considered. They were used to obtain the regression models of the crashworthiness of the segmented tubes (Table 1).

2.2 Crashworthiness parameters

Based on the literature review (Souzangarzadeh et al. 2017; Song et al. 2013), appropriate responses including absorbed energy (E^j), initial peak load (F_i^j), maximum crush load (F_{max}^j that $j = 0^\circ, 15^\circ, \text{ and } 30^\circ$), and mass of the structure (M)

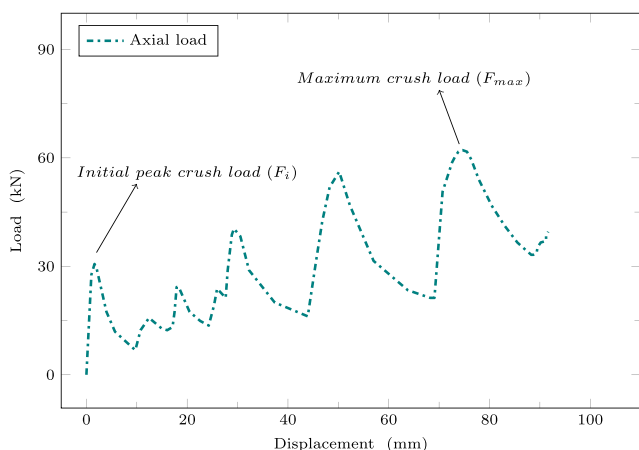


Fig. 3 Typical crushing progress curve of a cylindrical segmented tube (Jandaghi Shahi and Marzbanrad 2012)

were chosen to evaluate the effectiveness of the tubes during crushing under three loading angles ($0^\circ, 15^\circ, \text{ and } 30^\circ$).

2.2.1 Absorbed energy

The absorbed energy is defined as the area under the load-displacement response curve:

$$E = \int F d\delta \tag{2}$$

where F is the crushing force and δ the crushing distance.

2.2.2 Initial and maximum peak crushing loads

The load-displacement curve of the segmented tubes (as shown in Fig. 3) consists of the initial peak load (F_i) and the maximum peak load (F_{max}). However, the initial peak

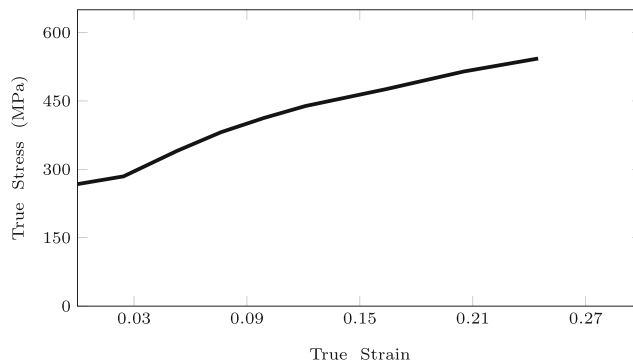


Fig. 4 The true stress-strain curve for the mild steel (Rezvani 2017)

Table 2 Material properties of the mild steel (Rezvani 2017)

Density	Young's modulus	Yield stress	Ultimate stress	Poisson's ratio
7800 kg/m ³	210 GPa	265 MPa	421 MPa	0.29

Fig. 5 Simulation of the cylindrical segmented tube under axial and oblique loadings

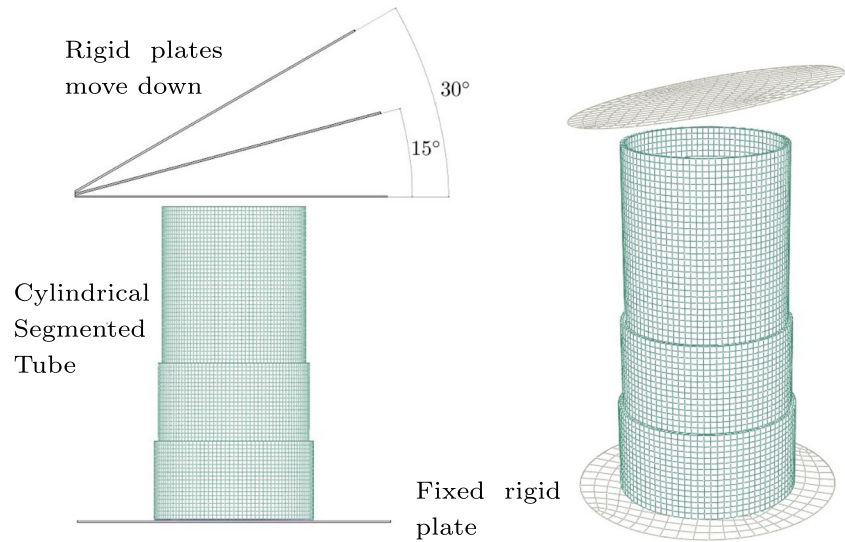
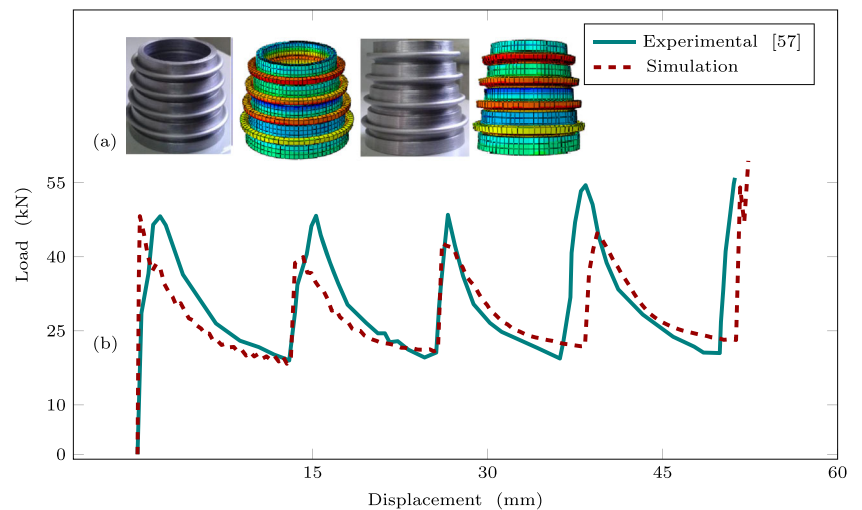


Table 3 Applied element types for each part of simulation in the FEM modelling

Parts	Element type	Element size
Segmented tube	Solid elements, C3D8R (an 8-node linear brick, reduced integration, hourglass control)	1.5 mm
Upper and lower plates	Rigid elements, R3D4 (A 4-node 3-D bilinear rigid quadrilateral)	2 mm

Fig. 6 The response curve of the numerical model in the present work and that of experimental work (Rezvani (Rezvani 2017)) for conically stiffened tubes with annular rings under axial crush, **a** Deformation mode. **b** Load-displacement behavior



load occurs at the onset of the crushing progress and the maximum peak load occurs at the end of the curve before any densification. The present study aims to optimize the segmented circular tube to have the lowest F_i and F_{max} while realizing the highest and lowest amount of the energy absorption and structure weight, respectively.

2.3 Material properties

The FEM model material properties, mild steel alloy, were derived from a standard tensile test according to Rezvani (2017). Figure 4 shows the approximated true stress-strain data points used in the numerical simulations. Furthermore, Table 2 lists the material properties of the mild steel.

2.4 Simulation

To obtain all the design point responses of the segmented tubes according to Table 1, the FEM using explicit FE code ABUS/CAE version 6.5 was employed. All the tubes were modeled as a 3D solid model and simulated under axial and oblique loads according to Section 2.2. Each tube was loaded via shifting downward the top rigid plate with a constant velocity of 80 mm/min, while being constrained in all degrees of freedom by the bottom plate (Fig. 5). The general contact algorithm with a friction coefficient of 0.2 was chosen to simulate the contact of the tube walls' elements with the plates and each other during the collapse of tubes. Table 3 indicates the features of the elements employed after convergence, which produced acceptable results in reasonable computational time. All sampling points were simulated on a CORE i7-6700HQ @ 2.6 GHz with 13 ± 3 min of CPU-Time for each simulation.

2.5 Finite element model validation

Rezvani (2017) experimentally investigated the crush behavior of conically stiffened mild steel tubes with annular rings under axial loading. As Fig. 6 shows, the experimental load-displacement curve agrees with the simulation of the same structure realized here for validation purposes. Furthermore, Table 4 presents the detailed comparison of the numerical and experimental results. Accordingly, the FEM model may be employed to simulate the crushing of the segmented tubes with a similar high accuracy.

2.6 Crashworthiness optimization

2.6.1 D-Optimal custom designs

RSM D-optimal design was utilized with the help of the FEM to develop the response surface (RS) models. D-optimal designs are one form of design of experiments

Table 4 The comparison of the experimental results for conically stiffened with annular rings mild steel tubes with the numerical simulation results (Rezvani 2017)

	Experimental (Rezvani 2017)	Numerical	Error
Initial peak load	48.4 kN	48.2 kN	0.4%
Absorbed energy	1.52 kJ	1.48 kJ	3.0%

generated by a computer algorithm. Standard classical designs such as full factorials estimate the effects of all factors and their interactions, while the fractional factorials screen the important factors. The latter, a design with a carefully chosen fraction of points often has the preferable properties of being both balanced and orthogonal (Montgomery 2017). On the other, D-optimal design matrices are usually not orthogonal, and effect estimates are correlated. It can also formulate the responses with a low number of required design points. Meanwhile, the method often helps to reach a model with acceptable quality. Another reason for employing D-optimal designs instead of standard classical designs is the complexity of design space (e.g., when there are constraints on factor settings, which cannot be handled by classical methods) (Kovach and Cho 2009).

The energy absorption responses can be related to the design variables by the following models. They specifically provide a prediction of responses based on geometrical parameters of multi-segmented tube. They can also assess the influence of the above parameters on the structure crashworthiness response variables. In the end, the verified regression models will be employed in a multi-objective optimization framework to select the best tube design. Thirty-four runs of experiments (Table 1) were conducted, with their levels for five independent variables shown in Fig. 2, where $L_1 + L_2 + L_3 = L_{Total} = 120$ mm. Statistical software, design-expert V7, was used to apply RSM D-optimal design on the outcomes of the FEM models. In order to improve regression models, according to Fig. 1, any achieved optimum tubes regression outcome was compared to FEMs; if the contrast between the outcomes of regression and FEM was unacceptable with a disagreeable error, a custom design point was added to the design points. After that, the DOE was regenerated to have better regression models. These measures were repeated until all the outcomes were acceptable. Therefore, twenty more runs were added to the whole runs to construct the final regression models (details of these models will be presented in Section 3.1.1).

2.6.2 Multi-objective optimization

As a general rule to design energy absorbers in automotive applications, the amount of absorbed energy (E) should

be as high as possible, while the transmitted force to other parts of the vehicle or occupants is as low as possible. According to Section 2.2, in typical thin-walled tubes, the initial peak load (F_i) is usually the same as the maximum peak load (F_{max}); however, in multi-segmented structures, they can be different (Fig. 3). Thus, both F_i and F_{max} are used as the force indicators in this study. Also, as the typical accidents are not always axial, the energy and force indicators of off-axial loads (15° and 30°) were also considered. Furthermore, the structure should remain light in terms of weight. To this end, these indicators as objective functions were considered contradicting objectives that are to be minimized and/or maximized at once. Thus, the optimization problem of the cylindrical segmented tubes under oblique loadings was formulated as follows:

$$\left\{ \begin{array}{l} \text{Minimize} \left\{ \begin{array}{l} f_1 = F_i^0(x) \\ f_2 = F_i^{15}(x) \\ f_3 = F_i^{30}(x) \end{array} \right. \\ \text{Minimize} \left\{ \begin{array}{l} f_4 = F_{max}^0(x) \\ f_5 = F_{max}^{15}(x) \\ f_6 = F_{max}^{30}(x) \end{array} \right. \\ \text{Maximize} \left\{ \begin{array}{l} f_7 = E^0(x) \\ f_8 = E^{15}(x) \\ f_9 = E^{30}(x) \end{array} \right. \\ \text{Less is better } f_{10} = M(x) \\ \text{S.t } x^l \leq x \leq x^u \end{array} \right. \quad (3)$$

where, the design variables are $x = (L_1, L_2, L_3, t_1, \text{ and } t_c)$; and x^l and x^u indicate the limits of the design variables (4). It is worth mentioning that the custom design points added to Section 2.6.1 had a wider range. Therefore, the constraints were updated accordingly in (4). To solve this optimization problem, the derived regression models by RSM D-optimal design were used.

$$\left\{ \begin{array}{l} L_1 : 15 \leq x \leq 75 \text{ mm} \\ L_2 : 15 \leq x \leq 75 \text{ mm} \\ L_3 : 15 \leq x \leq 75 \text{ mm} \\ t_1 : 1 \leq x \leq 1.9 \text{ mm} \\ t_c : 0.25 \leq x \leq 0.95 \text{ mm} \\ \text{where } L_1 + L_2 + L_3 = 120 \text{ mm} \end{array} \right. \quad (4)$$

2.7 Selection

The process of selecting appropriate materials and structures within optimum product design paradigm plays an essential role (Jahan et al. 2016). Moreover, without a standard multi-criteria selection technique, results of utilitarian engineering designs may be rejected. In the present study, in the interest of selecting an efficient overall design for the cylindrical segmented tubes, after creation of Pareto solutions from optimization problem of Eqs. 3 and 4, an integration of MULTIMOORA and combinative weighting

(CW) method was used as a hybrid MADM method. The applied strategy was named CW-MULTIMOORA.

2.7.1 The combinative weighting (CW) method

Jahan et al. (2012) proposed the CW method as a new weighting technique to combine different weighting methods. In a case study, CW combined three different weighting methods: entropy as an objective method, AHP as a subjective method, and correlation weights. The method makes adequate provision for designers as decision-makers in complex decision-making scenarios. In comparison with classical approaches, the correspondence between attributes in CW is more realistic, and incorporation of various weights can aid to avoid a subjectivity of criteria weighting, specially by inexperienced decision-makers. To define the importance of attributes/responses, the CW method is composed of the following steps:

Step one: Calculate the entropy as the objective weighting method

To reduce personal bias in designing products, the Entropy idea can be employed as an objective weighting strategy. The Entropy idea has been effectively applied in different decision-making processes (Jahan et al. 2016). The attributes having a distinctive difference from other attributes gain higher importance, owing to their more influence on the final ranking results. The responses of the alternatives to the attribute are first presented in a decision matrix of X (5), where m and n indicate the number of alternatives and attributes, respectively.

$$X = [x_{ij}]_{m \times n} \quad i = 1, 2, \dots, m \text{ and } j = 1, 2, \dots, n \quad (5)$$

The weight of attributes via the Entropy method is determined by

$$p_{ij} = \frac{x_{ij}}{\sum_{i=1}^m x_{ij}}, \quad i = 1, \dots, m \text{ and } j = 1, \dots, n \quad (6)$$

$$E_{ij} = \frac{-\sum_{i=1}^m p_{ij} \ln(p_{ij})}{\ln(m)}, \quad j = 1, \dots, n \quad (7)$$

$$w_j^o = \frac{1 - E_j}{\sum_{k=1}^n (1 - E_k)}, \quad j = 1, \dots, n \quad (8)$$

where p_{ij} is the project outcomes as the normalization of the decision matrix. And E_{ij} is entropy measure of the p_{ij} to obtain objective weights (w_j^o).

Step two: Implement the numeric logic (NL) as a subjective method

The subjective methods determine the weight of attributes solely based on the preference information of the attributes given by a specialist or designer. To determine the weight of attributes in the numeric logic (NL), as a pair-wise comparison method, every two attributes

Table 5 Summarized table for the steps of CW method

Methods	Weighting strategies		Formula
Entropy	Objective weighting	w_j^o	$\frac{1 - E_j}{\sum_{k=1}^n (1 - E_k)}$ (8)
Numeric logic	Subjective weighting	w_j^s	$\frac{\sum_{k=1}^n C_{jk}}{\sum_{j=1}^n \sum_{k=1}^n C_{jk}}$ (9)
Correlation's effect		w_j^c	$\frac{\sum_{k=1}^n (1 - R_{jk})}{\sum_{j=1}^n (\sum_{k=1}^n (1 - R_{jk}))}$ (11)
Combinative weighting		w_j	$\frac{(w_j^o w_j^s w_j^c)^{1/3}}{\sum_{j=1}^n (w_j^o w_j^s w_j^c)^{1/3}}$ (12)

should be compared relatively and receive their importance numerically. The first attribute (C_{jk}) obtains any figure between 0 and 1 (0 means the lowest priority and 1 means the highest priority) as weight; moreover, the weight of the other attribute is $C_{kj} = 1 - C_{jk}$. Subsequently, the final importance weight of each attribute can be calculated (Alemi-Ardakani et al. 2016):

$$w_j^s = \frac{\sum_{k=1}^n C_{jk}}{\sum_{j=1}^n \sum_{k=1}^n C_{jk}}, j \text{ and } k = \{1, \dots, n\} \text{ and } j \neq k \quad (9)$$

Step three: Calculate weight of correlation's effect

The concept of the effect of correlation on the weights is concerned with the following situation: the high correlation of attributes with other attributes should lead them to be less important due to function of other attributes.

$$R_{jk} = \begin{cases} \frac{\sum_{i=1}^m (x_{ij} - \bar{x}_j)(x_{ik} - \bar{x}_k)}{\sqrt{\sum_{i=1}^m (x_{ij} - \bar{x}_j)^2 \sum_{i=1}^m (x_{ik} - \bar{x}_k)^2}}, & \text{For positively correlated attributes} \\ -\frac{\sum_{i=1}^m (x_{ij} - \bar{x}_j)(x_{ik} - \bar{x}_k)}{\sqrt{\sum_{i=1}^m (x_{ij} - \bar{x}_j)^2 \sum_{i=1}^m (x_{ik} - \bar{x}_k)^2}}, & \text{For negatively correlated attributes} \end{cases} \quad (10)$$

$$w_j^c = \frac{\sum_{k=1}^n (1 - R_{jk})}{\sum_{j=1}^n (\sum_{k=1}^n (1 - R_{jk}))}, j = 1, \dots, n \quad (11)$$

where R_{jk} , x_{ij} , w_j^c , and \bar{x} are the correlation coefficient values, elements of the decision matrix, correlation weights, and the mean values of a column of the decision matrix, respectively.

Step four Combine the weights

To combine the weights from the above weighting methods, the following equation has been suggested by Jahan et al. (2012), where w_j^o , w_j^s , and w_j^c are the objective, subjective, and correlation weights, respectively.

$$w_j = \frac{(w_j^o w_j^s w_j^c)^{1/3}}{\sum_{j=1}^n (w_j^o w_j^s w_j^c)^{1/3}}, j = 1, \dots, n \quad (12)$$

2.7.2 MULTIMOORA approach

Brauers and Zavadskas (2010) and Brauers and Zavadskas (2012) proposed the MULTIMOORA approach, as a robust multi-criteria decision-making method. It consists of three ranking systems: ratio system, the reference point approach, and the full multiplicative form. The MULTIMOORA method has been widely used in such different selection problems as mining selection (Liang et al. 2018), robot

selection (Liu et al. 2019), risk evaluation (Zhao et al. 2016; Fattahi and Khalilzadeh 2018), ranking and selection of the advantageous performance appraisals for organizations (Ijadi Maghsoodi et al. 2018), selection of the residential house construction elements and materials (Zavadskas et al. 2017), hospital leanness evaluation (Abdi 2018), and also selection of an optimal power battery recycling mode (Ding and Zhong 2018). MULTIMOORA has also been extended to become more flexible in solving high-risk MADM problems (Zavadskas et al. 2015; Hafezalkotob et al. 2016b; Stanujkic et al. 2017). Hafezalkotob and Hafezalkotob (Hafezalkotob and Hafezalkotob 2016) extended the MULTIMOORA method based on the Shannon entropy concept. Their suggested model had two frameworks: the entropy weighting and the weighted MULTIMOORA. The weighted MULTIMOORA is also employed in this study based on the following procedure. To make the decision matrix dimensionless and comparable under different design criteria, Brauers and Zavadskas (2006) recommended the following equation to normalize the decision matrix (5):

$$x_{ij}^* = \frac{x_{ij}}{[\sum_{i=1}^m x_{ij}^2]^{1/2}} \quad (13)$$

Also, the combinative weighting (CW) method was employed as a weighting technique to define the importance of the attributes, i.e., w_j .

First part of MULTIMOORA: *The ratio system*

The normalized decision matrix, i.e., x_{ij}^* , multiplied by CW weights, is used to find the deviation of the beneficial attributes from the non-beneficial ones (14), where the g and n are the number of beneficial attributes and the total number of attributes, respectively. Afterwards, the score values of y_i^w are ascendantly sorted to obtain the best alternative (Hafezalkotob and Hafezalkotob 2016) (Table 5).

$$y_i^w = \sum_{j=1}^g w_j x_{ij}^* - \sum_{j=g+1}^n w_j x_{ij}^* \tag{14}$$

$$A_{WRS}^* = \{A_i | = \max_i y_i^w\} \tag{15}$$

Second part of MULTIMOORA: *The reference point system*

This system is computed by defining a reference point vector (16) and computing its deviation from the normalized rating (17). Moreover, the CW weighting method was added here to the reference point approach (18). Based on the reference point approach, the best alternative should have the minimum score value of z_i^w (19) (Hafezalkotob and Hafezalkotob 2016).

$$r_j = \begin{cases} \max_i x_{ij}^*, & j \leq g, \\ \min_i x_{ij}^*, & j > g. \end{cases} \tag{16}$$

$$d_{ij} = (r_j - x_{ij}^*) \tag{17}$$

$$z_i^w = \max_j w_j d_{ij} \tag{18}$$

$$A_{WRP}^* = \{A_i | = \min_i z_i^w\} \tag{19}$$

Third part of MULTIMOORA: *The full multiplicative*

The numerical value of this scoring system weighted by the CW as the exponents is obtained by (20). Then, the best alternative can be determined (Hafezalkotob and Hafezalkotob 2016):

$$U_i^w = \frac{\prod_{j=1}^g (x_{ij}^*)^{w_j}}{\prod_{j=g+1}^n (x_{ij}^*)^{w_j}} \tag{20}$$

$$A_{WMF}^* = \{A_i | = \max_i U_i^w\} \tag{21}$$

Final ranking: To summarize and conjoin all the above three ranking systems (from 14, 18, and 20), the dominance theory, as the final ranking scheme, can be utilized (Brauers and Zavadskas 2011).

3 Results and discussion

3.1 Analysis and validation of D-optimal models

The outcomes of DOE with the aid of the design-expert software could provide an analysis to evaluate the performance of different segmented tube structures. At first, each response model needed to be transformed to meet normality assumption of standard regression. Figure 7, that extracted from the software, is a general guideline, set by the natural log of the sum of squares of the residuals, used to select the proper power law transformation based on lambda (λ). The minimum point on the Box-Cox curve indicates the lambda: inverse (if $\lambda = -1$), natural log (if $\lambda = 0$), square root (if $\lambda = 0.5$), and no transformation (if $\lambda = 1$). Table 6 shows the differences between the analysis of variance of non-transformed and transformed values of the responses. It can be seen that the transformation leads to more accurate

Fig. 7 Example of Box-Cox plot of $F_{max}^{30} (f_8)$ for power transforms

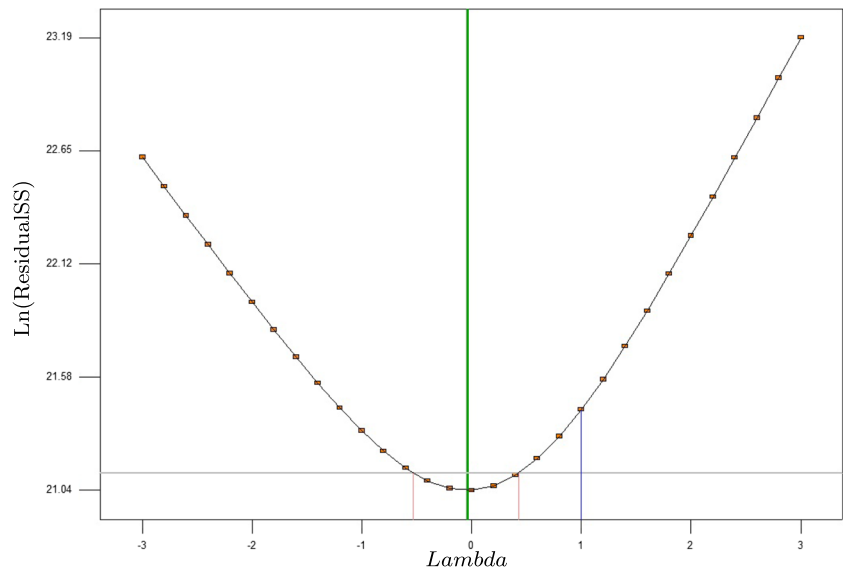


Table 6 The ANOVA example table of $F_{max}^{30}(f_8)$ for non-transformed and after transforming based on Log

Factors	F Value	P value		
L_1	31.21	< 0.0001	R-Squared	0.9115
L_2	38.06	< 0.0001	Adj R-Squared	0.9020
t_1	240.78	< 0.0001	Pred R-Squared	0.8899
t_c	146.56	< 0.0001	Adeq Precision	35.169
$L_1 t_c$	5.69	0.0212	Transformation	None
L_1	41.840	< 0.0001	R-Squared	0.9312
L_2	47.510	< 0.0001	Adj R-Squared	0.9239
t_1	322.910	< 0.0001	Pred R-Squared	0.9143
t_c	194.520	< 0.0001	Adeq Precision	40.136
$L_1 t_c$	4.600	0.0371	Transformation	Log

regression model. The sample plot of the actual versus the predicted values of response (Fig. 8) can detect points that the model cannot 100% accurately predict. The response values should be ideally split by the 45-degree line. The normal probability graph (Fig. 9) demonstrates whether the residuals follow a normal distribution; the points should follow a straight line.

It was indicated by the analysis section in design-expert software that linear, 2FI, and quadratic models are statistically recommended for the attributes. The adequacy of the regression models and the variance for attributes were checked, analyzed, and summarized in Table 7. Accordingly, each model F value and the model P value of < 0.0001 could specify the significance and a low chance of the noise in the prediction, respectively. The analysis revealed that the contrast between the predicted and adjusted R-squared is less than 0.20, which is acceptable. The Adeq Precision value indicated the signal to noise ratio, which should be greater than 4. The mentioned evidence suggested that all the nine models

could be employed in the subsequent optimizing process. Table 8 illustrates the outcomes of the numerical simulations, predicted values, and the relative error.

3.1.1 Effect of geometrical factors on the design responses

Table 9 summarizes the most effective factors/design variables employed to formalize each response. P value plays a vital role in indicating the impact of each factor in each response, namely the factors with P values less than 0.05 could be kept remained in the model. Furthermore, the table shows the final regression models in terms of design variables. F values are indicative of the order of the factors' influence on the response. To have a general perspective of the influence of design variables, a relative F value ratios ($= \frac{F\ value^i}{F\ value_{max}^j}$, i : design variable, j : response) of each design variable were compared (Fig. 10).

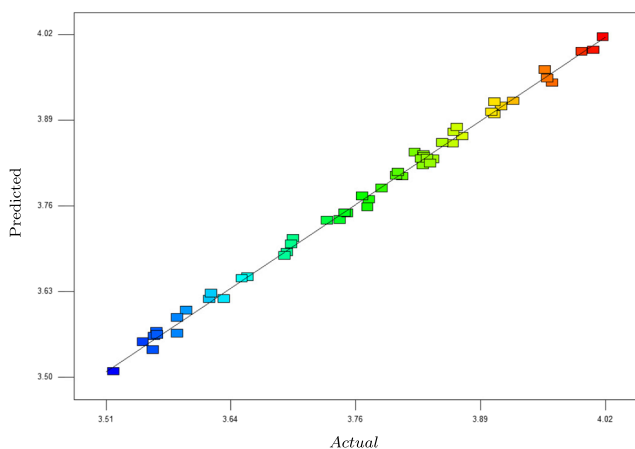


Fig. 8 The actual versus the predicted values after the transformation of $E^{15}(f_6)$ based on Log

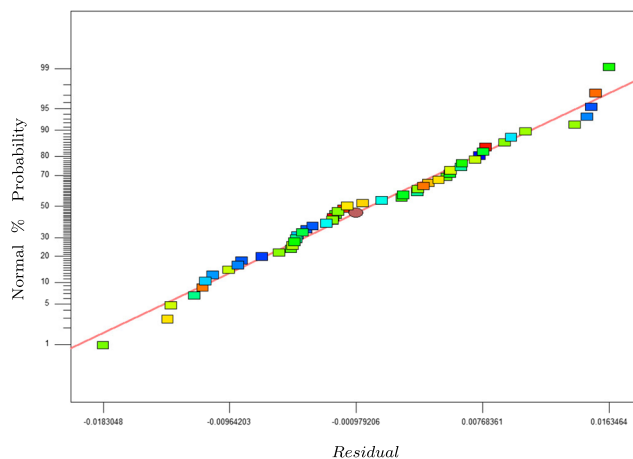


Fig. 9 Normal plot of the residuals after the transformation of $E^{15}(f_6)$ based on Log

Table 7 The summary of analysis of variances of models for the segmented tube design responses

Responses	Model	<i>F</i> value	<i>P</i> value	<i>R</i> ²	Adj <i>R</i> ²	Pred <i>R</i> ²	Adeq Precision
<i>f</i> ₁	2FI	211.57	< 0.0001	0.9283	0.9239	0.9143	33.576
<i>f</i> ₂	2FI	78.86	< 0.0001	0.8935	0.8822	0.8629	29.251
<i>f</i> ₃	2FI	165.43	< 0.0001	0.9462	0.9405	0.9289	44.756
<i>f</i> ₄	Quadratic	2007.76	< 0.0001	0.9962	0.9957	0.9949	109.087
<i>f</i> ₅	2FI	85.13	< 0.0001	0.9006	0.8900	0.8741	33.446
<i>f</i> ₆	Quadratic	769.08	< 0.0001	0.9961	0.9948	0.9928	100.821
<i>f</i> ₇	Linear	242.80	< 0.0001	0.9066	0.9029	0.8974	37.473
<i>f</i> ₈	2FI	127.25	< 0.0001	0.9312	0.9239	0.9143	40.136
<i>f</i> ₉	2FI	501.43	< 0.0001	0.9917	0.9897	0.9864	81.131

Effect of thickness parameters on responses It can be seen in Fig. 10 that the two thickness parameters (*t*₁ and *t*₂) are the most influential factors. In this regard, *t*₁, as a thickness of the first segment of the tube, is the key parameter varying all response functions; the relative *F* value ratios of *t*₁ of the nine responses are equal to 1.

Effect of length parameters on responses Figure 10 shows that the nine response function design is less dependent on the tube segments' length than the thickness factors. Moreover, *L*₁, the length of the first segment, has a higher effect on the absorbed energy responses than the second segment's length, *L*₂. The regression models of *F*_{*i*} (*f*₁, *f*₄, and *f*₇) can be independent of the length of segments, since *L*₁ has insignificant effect only on *F*_{*i*}¹⁵ (*f*₄), and *L*₂ has no effect on them. Interestingly, the second order of *t*₁ and *t*₂ has more *F* values than *L*₁ (Table 9), which means the effect of *L*₁ on the model is almost negligible.

3.2 Multi-objective optimization

Table 10 shows the resulting fifteen Pareto front points, obtained through design-expert software by employing regression models of nine response functions (Table 9) and

the mass formula ($M = \rho \times v$) for the structures' weight. Each solution is based on a particular scenario, having a different fusion of responses, where the responses of each group have equal weights (Table 10). It can be seen that the responses not employed in each scenario were left blank. The selection method could sort the solutions of different responses' fusions based on the designer's preferences. The first tube in the table was optimized based on all ten responses (*f*₁→*f*₁₀). The energy response was combined with either of the forces (*F*_{*i*} or *F*_{max}) in the third, fourth, and fifth scenarios. The sixth, seventh, and tenth tubes were optimized based on only one response (*F*_{*i*} or *F*_{max} or *E*) under three loads; scenarios 2, 8, and 9 considered weight as well. The eleventh and twelfth scenarios optimized only force responses. The thirteenth, fourteenth, and fifteenth tubes were optimized based on ordinary responses (*F*_{*i*}, *F*_{max}, *E*, and mass). Moreover, the basic tube, i.e., with no segmentation, was considered to be optimum when the only design parameter to be optimized is thickness (*t*₁).

3.3 Selection results

The most sufficient energy absorber design was selected among the candidates that were obtained from optimization in Table 10. The MULTIMOORA method sorted candidate

Table 8 The comparison between the predicted values by the D-optimal DOE and those of the numerical simulations

	<i>f</i> ₁ <i>F</i> _{<i>i</i>} ⁰ kN	<i>f</i> ₂ <i>F</i> _{Max} ⁰ kN	<i>f</i> ₃ <i>E</i> ⁰ kJ	<i>f</i> ₄ <i>F</i> _{<i>i</i>} ¹⁵ kN	<i>f</i> ₅ <i>F</i> _{Max} ¹⁵ kN	<i>f</i> ₆ <i>E</i> ¹⁵ kJ	<i>f</i> ₇ <i>F</i> _{<i>i</i>} ³⁰ kN	<i>f</i> ₈ <i>F</i> _{Max} ³⁰ kN	<i>f</i> ₉ <i>E</i> ³⁰ kJ
REG*	54.88	64.44	2.65	15.83	49.90	3.00	4.05	36.73	1.93
FEM**	55.15	61.35	2.76	16.73	51.11	3.32	3.91	38.76	1.95
Error%	0.49	5.04	3.82	5.36	2.37	9.51	3.70	5.23	1.16

*Regression models

**Finite element method

Table 9 The ANOVA of design factors for each response (objective function)

Responses	Factors	<i>F</i> value	<i>P</i> value	Final equation
<i>f</i> ₁	<i>t</i> ₁	594.629	< 0.0001	$10^{(+4.16996+0.57713 \times t_1)}$
	<i>t</i> _{<i>c</i>}	20.446	< 0.0001	$+0.22260 \times t_c - 0.25329 \times t_1 \times t_c$
	<i>t</i> ₁ <i>t</i> _{<i>c</i>}	10.213	0.0024	
	<i>L</i> ₁	17.030	0.0001	
	<i>L</i> ₂	19.530	< 0.0001	$10^{(4.49370-2.26674E-3 \times L_1)}$
<i>f</i> ₂	<i>t</i> ₁	170.530	< 0.0001	$-2.21568E-3 \times L_2 + 0.42023 \times t_1$
	<i>t</i> _{<i>c</i>}	141.450	< 0.0001	$+0.78968 \times t_c - 0.27190 \times t_1 \times t_c$
	<i>t</i> ₁ <i>t</i> _{<i>c</i>}	8.690	0.005	
	<i>L</i> ₁	65.894	< 0.0001	
	<i>L</i> ₂	31.996	< 0.0001	$10^{(3.10313-3.69279E-3 \times L_1)}$
<i>f</i> ₃	<i>t</i> ₁	468.696	< 0.0001	$-2.34881E-3 \times L_2 + 0.51899 \times t_1$
	<i>t</i> _{<i>c</i>}	204.036	< 0.0001	$+0.78189 \times t_c - 0.26789 \times t_1 \times t_c$
	<i>t</i> ₁ <i>t</i> _{<i>c</i>}	12.303	0.0010	-0.5
	<i>L</i> ₁	16.760	0.0002	
	<i>t</i> ₁	11516.12	< 0.0001	$7791.44257 + 25.65624 \times L_1$
<i>f</i> ₄	<i>t</i> _{<i>c</i>}	66.050	< 0.0001	$+2592.31284 \times t_1 - 13509.02686 \times t_c$
	<i>L</i> ₁ <i>t</i> ₁	5.590	0.0224	$-35.12493 \times L_1 \times t_1 + 8462.03334 \times t_1^2$
	<i>t</i> ₁ ²	33.790	< 0.0001	$+15042.91648 \times t_c^2$
	<i>t</i> _{<i>c</i>} ²	25.320	< 0.0001	
	<i>L</i> ₁	67.035	< 0.0001	
	<i>L</i> ₂	57.381	< 0.0001	$(+200.80995 - 0.48088 \times L_1$
	<i>t</i> ₁	139.917	< 0.0001	$-1.34313 \times L_2 + 86.49449 \times t_1$
<i>f</i> ₅	<i>t</i> _{<i>c</i>}	127.804	< 0.0001	$+214.16763 \times t_c - 1.96101 \times L_1 \times t_c)^2 - 0.5$
	<i>L</i> ₁ <i>t</i> _{<i>c</i>}	6.955	0.0113	
	<i>L</i> ₁	860.650	< 0.0001	
	<i>L</i> ₂	362.301	< 0.0001	$10^{(+2.73148+6.02635E-3 \times L_1)}$
	<i>t</i> ₁	4212.581	< 0.0001	$+2.95477E-3 \times L_2 + 0.72982 \times t_1$
	<i>t</i> _{<i>c</i>}	2407.733	< 0.0001	$+0.85776 \times t_c - 8.22871E-5 \times L_1 \times L_2$
	<i>L</i> ₁ <i>L</i> ₂	35.602	< 0.0001	$+1.65888E-3 \times L_1 \times t_1 - 5.17772E-3 \times L_1 \times t_c$
	<i>L</i> ₁ <i>t</i> ₁	31.513	< 0.0001	$+1.47904E-3 \times L_2 \times t_1$
	<i>L</i> ₁ <i>t</i> _{<i>c</i>}	119.451	< 0.0001	$-2.64020E-3 \times L_2 \times t_c$
	<i>L</i> ₂ <i>t</i> ₁	27.475	< 0.0001	$-0.15502 \times t_1 \times t_c$
<i>f</i> ₆	<i>L</i> ₂ <i>t</i> _{<i>c</i>}	29.078	< 0.0001	$-6.98066E-5 \times L_1^2$
	<i>t</i> ₁ <i>t</i> _{<i>c</i>}	76.811	< 0.0001	$-2.85869E-5 \times L_2^2$
	<i>L</i> ₁ ²	34.682	< 0.0001	$-0.18214 \times t_1^2$
	<i>L</i> ₂ ²	10.249	0.0027	
	<i>t</i> ₁ ²	49.527	< 0.0001	
	<i>t</i> ₁	461.180	< 0.0001	$-2573.79799 + 5947.42755 \times t_1$
	<i>t</i> _{<i>c</i>}	38.720	< 0.0001	$+2724.15487 \times t_c$
	<i>L</i> ₁	41.840	< 0.0001	
	<i>L</i> ₂	47.510	< 0.0001	$10^{(+4.37940-7.29456E-4 \times L_1)}$
	<i>f</i> ₈	<i>t</i> ₁	322.910	< 0.0001
<i>t</i> _{<i>c</i>}		194.520	< 0.0001	$+0.47567 \times t_c - 3.28117E-3 \times L_1 \times t_c$
<i>L</i> ₁ <i>t</i> _{<i>c</i>}		4.600	0.0371	
<i>L</i> ₁		563.738	< 0.0001	
<i>L</i> ₂		233.705	< 0.0001	$10^{(+3.19845-4.93835E-3 \times L_1)}$
<i>t</i> ₁	2588.466	< 0.0001	$-3.11554E-3 \times L_2 + 0.21126 \times D$	

Table 9 (continued)

Responses	Factors	F-value	P-value	Final equation
f_9	t_c	834.397	< 0.0001	$+0.77206 \times t_c + 3.54032E-5 \times L_1 \times L_2$
	$L_1 L_2$	9.713	0.0033	$+2.13553E-3 \times L_1 \times t_1 - 5.96966E-3 \times L_1 \times t_c$
	$L_1 t_1$	25.188	< 0.0001	$+1.01007E-3 \times L_2 \times t_1$
	$L_1 t_c$	81.827	< 0.0001	$-3.53922E-3 \times L_2 \times t_c$
	$L_2 t_1$	6.117	0.0175	$-0.080585 \times t_1 \times t_c$
	$L_2 t_c$	27.866	< 0.0001	
	$t_1 t_c$	9.922	0.0030	

tubes in Table 10 from the worst to the best in terms of all ten responses and their weights, which are obtained via the CW method. The CW weights were acquired by a combination of three kinds of weighting methods: entropy as the objective weighting method, NL method as the subjective method (Table 11), and the weights of correlation effect (Table 12). Table 13 shows the eventual weights used in the decision-making process. Table 14 presents the predicted attributes/responses and the ranking results of the CW-MULTIMOORA method for the fifteen segmented tubes (Table 10). Furthermore, for the sake of comparisons, an optimum basic tube was added as a candidate in the selection process. The selected candidate, number 4, was obtained by the final rank. This tube had a thickness of 1 mm and the thickness factor of 0.81. The lengths of the sections were 15, 30.12, and 74.78 mm, respectively (Table 10). In addition, it can be observed that the basic tube is the worst

design among others. As mentioned earlier, optimizing energy absorbers is often carried out by considering axial crushworthiness as responses (Taştan et al. 2016; Khalkhali et al. 2016; Song et al. 2013); here, tube 13 has been optimized based on only axial loading attributes (F_i^0 , F_{max}^0 , E^0 , and M) and obtained the seventh overall rank.

3.4 Load-displacement analysis

Figures 11, 12, and 13 show the load-displacement curves for basic and segmented tubes. As can be observed, in the basic tube whose thickness is constant, the load fluctuations along the tube length have an almost steady trend under axial loading (Fig. 11). On the other hand, in the segmented tube, while the wall thickness increases in terms of the thickness factor (t_c), the load curve grows. Therefore, in the course of the formation of the first fold, the first peak load is

Fig. 10 The comparison of the design variables' F value ratios

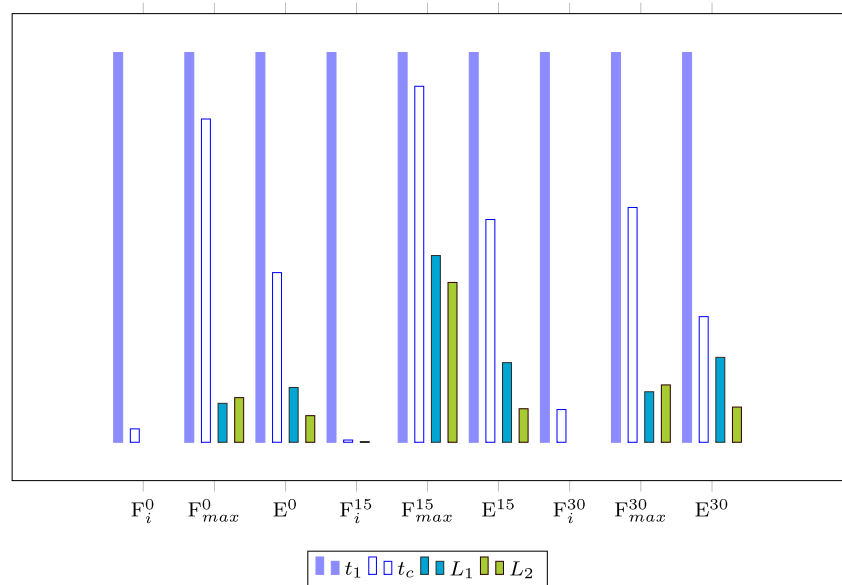


Table 10 Scenarios chosen for pareto front generation

	Design variables					Output responses									
	L_1 mm	L_2 mm	L_3 mm	t_1 mm	t_c	f_1 F_i^0	f_2 F_{max}^0	f_3 E^0	f_4 F_i^{15}	f_5 F_{max}^{15}	f_6 E^{15}	f_7 F_i^{30}	f_8 F_{max}^{30}	f_9 E^{30}	f_{10} M
1*	23.59	34.34	62.07	1	0.51	✓	✓	✓	✓	✓	✓	✓	✓	✓	✓
2	23.91	25.81	70.28	1.05	0.9	–	–	✓	–	–	✓	–	–	✓	✓
3	38.91	37.82	43.27	1	0.9	✓	–	✓	✓	–	✓	✓	–	✓	✓
4	15	30.12	74.88	1	0.81	✓	–	✓	✓	–	✓	✓	–	✓	–
5	26.89	74.99	18.12	1.88	0.25	–	✓	✓	–	✓	✓	–	✓	✓	–
6	14.21	40.82	64.97	1.9	0.8	–	–	✓	–	–	✓	–	–	✓	–
7	26.88	33.29	59.83	1	0.25	✓	–	–	✓	–	–	✓	–	–	–
8	39.07	63.12	17.81	1	0.25	✓	–	–	✓	–	–	✓	–	–	✓
9	26.04	56.06	37.9	1	0.25	–	✓	–	–	✓	–	–	✓	–	✓
10	56.74	48.23	15.03	1.14	0.25	–	✓	–	–	✓	–	–	✓	–	–
11	24.05	33.21	62.74	1	0.34	✓	✓	–	✓	✓	–	✓	✓	–	–
12	60.82	43.48	15.7	1	0.25	✓	✓	–	✓	✓	–	✓	✓	–	✓
13	15	31.9	73.1	1.01	0.36	✓	✓	✓	–	–	–	–	–	–	✓
14	48.03	16.34	55.63	1	0.55	–	–	–	✓	✓	✓	–	–	–	✓
15	41.27	41.82	36.91	1.32	0.25	–	–	–	–	–	–	✓	✓	✓	✓
16**	–	–	–	1.98	–	✓	✓	✓	✓	✓	✓	✓	✓	✓	✓

*Segmented tubes

**Basic tube

not the maximum crushing load of the whole tube crushing process.

Although it is hard to observe, the feature of the axial crushing of the basic tube in the off-axial load-displacement

curves, i.e., the maximum load is not equal to first peak load, the F_{max} of basic tube occurs sooner than the segmented tube under both oblique loads (Figs. 12 and 13). Although, the F_{max} of the segmented tubes is higher than that of the

Table 11 NL weighting results

Responses/ attributes	Relative numeric weights (C_{jk})									
	f_1	f_2	f_3	f_4	f_5	f_6	f_7	f_8	f_9	f_{10}
F_i^0	–	0.5	0.7	0.5	0.35	0.6	0.5	0.33	0.57	0.3
F_{max}^0	0.5	–	0.7	0.28	0.35	0.6	0.5	0.33	0.57	0.3
E^0	0.3	0.3	–	0.5	0.25	0.5	0.27	0.24	0.5	0.2
F_i^{15}	0.5	0.5	0.72	–	0.5	0.7	0.5	0.35	0.6	0.25
F_{max}^{15}	0.65	0.65	0.75	0.5	–	0.7	0.5	0.35	0.6	0.35
E^{15}	0.4	0.4	0.5	0.3	0.3	–	0.28	0.25	0.5	0.3
F_i^{30}	0.5	0.5	0.73	0.5	0.5	0.72	–	0.5	0.7	0.4
F_{max}^{30}	0.67	0.67	0.76	0.65	0.65	0.75	0.5	–	0.7	0.45
E^{30}	0.43	0.43	0.5	0.4	0.4	0.5	0.3	0.3	–	0.33
M	0.7	0.7	0.8	0.75	0.65	0.7	0.6	0.55	0.67	–
Weight (w^s)	0.1033	0.1033	0.1369	0.0973	0.0878	0.1282	0.0878	0.0711	0.1202	0.0640

Table 12 Weight of the criteria correlation

Responses/ attributes	R_{jk}									
	f_1	f_2	f_3	f_4	f_5	f_6	f_7	f_8	f_9	f_{10}
F_i^0	1	0.33	-0.47	0.9	0.19	-0.41	0.8	0.34	-0.41	0.52
F_{max}^0	0.33	1	-0.98	0.46	0.97	-0.98	0.52	0.98	-0.97	0.97
E^0	-0.47	-0.98	1	-0.59	-0.95	0.97	-0.62	-0.99	0.98	-0.99
F_i^{15}	0.9	0.46	-0.59	1	0.36	-0.56	0.97	0.5	-0.56	0.66
F_{max}^{15}	0.19	0.97	-0.95	0.36	1	-0.95	0.43	0.97	-0.96	0.93
E^{15}	-0.41	-0.98	0.97	-0.56	-0.95	1	-0.63	-0.96	0.98	-0.99
F_i^{30}	0.8	0.52	-0.62	0.97	0.43	-0.63	1	0.54	-0.61	0.7
F_{max}^{30}	0.34	0.98	-0.99	0.5	0.97	-0.96	0.54	1	-0.98	0.96
E^{30}	-0.41	-0.97	0.98	-0.56	-0.96	0.98	-0.61	-0.98	1	-0.98
M	0.52	0.97	-0.99	0.66	0.93	-0.99	0.7	0.96	-0.98	1
Weight (w^c)	0.0807	0.0865	0.1415	0.077	0.0898	0.1405	0.0773	0.0856	0.1403	0.0809

Table 13 Result of the combinative weights

	f_1 F_i^0	f_2 F_{max}^0	f_3 E^0	f_4 F_i^{15}	f_5 F_{max}^{15}	f_6 E^{15}	f_7 F_i^{30}	f_8 F_{max}^{30}	f_9 E^{30}	f_{10} M	Sum
w^o	0.0934	0.1046	0.1166	0.1103	0.1135	0.0838	0.106	0.0916	0.0982	0.0521	1
w^s	0.1033	0.1033	0.1369	0.0973	0.0878	0.1282	0.0878	0.0711	0.1202	0.0640	1
w^c	0.0807	0.0865	0.1415	0.077	0.0898	0.1405	0.0773	0.0856	0.1403	0.0809	1
w	0.0929	0.0986	0.1429	0.0947	0.0972	0.1157	0.0904	0.083	0.1194	0.0652	1

Table 14 The multi-objective design selection results

	f_1 F_i^0 kN	f_2 F_{max}^0 kN	f_3 E^0 kJ	f_4 F_i^{15} kN	f_5 F_{max}^{15} kN	f_6 E^{15} kJ	f_7 F_i^{30} kN	f_8 F_{max}^{30} kN	f_9 E^{30} kJ	f_{10} M kg	U_i^w	Ranks y_i^w	z_i^w	Final
1*	53.88	111.80	5.21	15.65	99.52	5.29	4.76	56.14	3.30	0.27	3	6	7	4
2	54.57	189.38	8.91	19.60	156.83	8.75	6.12	86.77	5.40	0.38	7	4	1	4
3	52.42	161.41	7.12	18.50	116.88	6.91	5.83	69.09	3.68	0.32	10	11	5	10
4	<u>52.75</u>	<u>170.84</u>	<u>8.17</u>	<u>17.63</u>	<u>151.54</u>	<u>7.78</u>	<u>5.58</u>	<u>80.99</u>	<u>5.27</u>	<u>0.36</u>	1	1	2	1
5	155.44	133.74	7.46	39.05	84.17	6.54	9.29	59.74	3.98	0.34	14	15	4	15
6	114.71	244.31	14.43	41.50	204.78	10.53	10.91	132.80	7.43	0.50	15	14	3	14
7	54.88	81.04	3.74	16.15	72.92	3.95	4.05	43.98	2.51	0.21	8	5	12	8
8	54.88	65.31	2.87	16.04	47.58	3.31	4.05	35.43	2.06	0.19	4	3	15	4
9	54.88	72.47	3.33	16.16	57.73	3.76	4.05	38.66	2.26	0.20	2	2	13	2
10	64.77	71.98	3.10	18.49	54.32	3.54	4.89	39.56	2.20	0.21	12	12	14	12
11	54.53	91.60	4.27	15.76	82.89	4.37	4.30	48.26	2.80	0.23	5	7	11	6
12	54.88	64.44	2.65	15.83	49.90	3.00	4.05	36.73	1.93	0.19	11	9	16	11
13	55.07	99.74	4.80	15.98	92.79	4.47	4.41	51.85	3.13	0.25	6	8	9	7
14	53.73	113.14	4.89	15.51	95.02	5.17	4.87	56.04	2.88	0.26	9	10	8	9
15	80.14	93.30	4.41	22.67	74.13	4.93	5.96	48.53	2.78	0.25	13	13	10	13
16**	107.41	107.41	5.82	44.73	84.84	6.27	13.26	55.37	3.82	0.32	16	16	6	16

* Regression models

** Finite element method

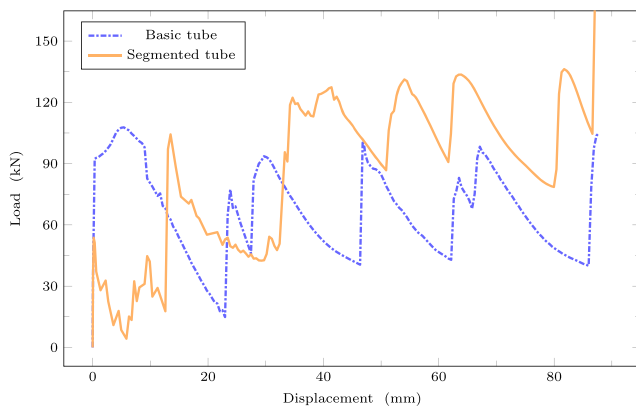


Fig. 11 Load-displacement curves of the selected cylindrical segmented tube and the basic tube under axial loading

basic tubes' under 15° and 30° loads, respectively, the first load of the segmented tube is much lesser (50–60%) than that of the basic tube. Furthermore, Table 15 shows an improvement of the energy absorber in the segmented tube (41%, 23%, and 39%) and a significant reduction in initial peak loads (59%, 79%, and 46%) in contrast to the basic tube. Eventually, the key feature of these tubes, lower initial peak load, remains comparable under the three loads.

Moreover, the load-displacement curve has an overall positive slope, resulting in an increasing trend of the energy absorption and reducing the aggressiveness in low-speed crashes of the vehicles (Nahas 1993). Figure 14 shows different stages of the axial and oblique crushes in the final selected cylindrical segmented tube during compression.

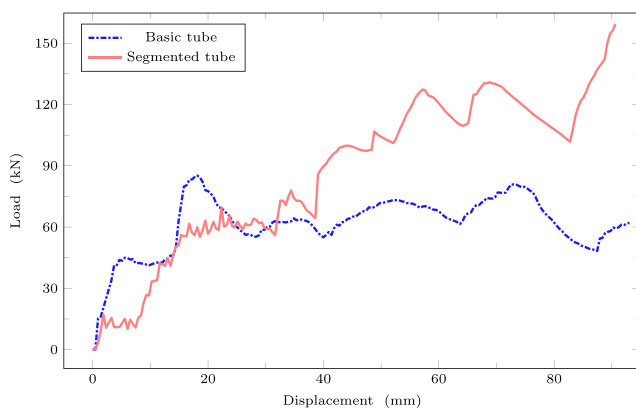


Fig. 12 Load-displacement curves of the selected cylindrical segmented tube and the basic tube under the oblique loading of 15°

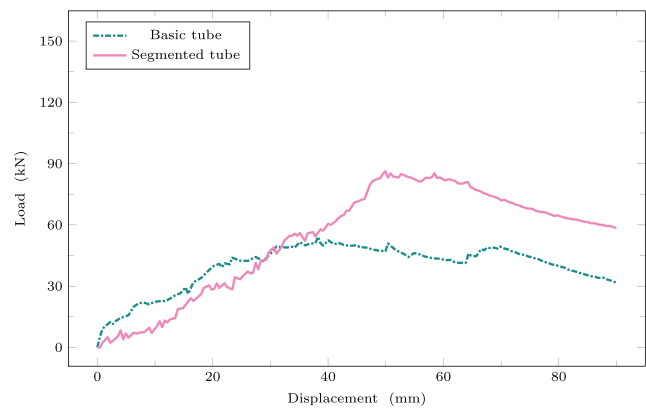


Fig. 13 Load-displacement curves of the selected cylindrical segmented tube and the basic tube under the oblique loading of 30°

4 Conclusion

In this article, the crashworthiness characteristics of the thin-walled cylindrical segmented mild steel tubes were investigated under axial and oblique loads. The most efficient candidate was found through the proposed combination of DOE and CW-MULTIMOORA. In line with this approach, the regression model of responses was achieved via D-optimal to predict the behavior of the tubes. The main conclusions from the study are:

- Aligned with the earlier studies (Souzangarzadeh et al. 2017; Jandaghi Shahi and Marzbanrad 2012), the segmented tube maintains its particular features: higher absorbed energy, lower initial peak load, and accruing the maximum load at the end of crushing. Additionally, the mentioned features continue to be satisfied under oblique loads.
- The comparison between the optimum basic tube and the selected segmented tube showed 41.4%, 23.8%, and 39.5% improvement in terms of the absorbed energy, respectively, under the axial load, 15° , and 30° loads. Furthermore, the initial peak loads yielded 50.8%, 60.6%, and 57.9% reduction under axial and two off-axial loadings, respectively.
- The CW-MULTIMOORA method arranged all the candidates from the best to the worst. The tube with the lengths of 15, 30.12, and 74.88 mm of L_1 , L_2 , and L_3 , respectively, with the first thickness (t_1) of 1 mm and the thickness factor (t_c) of 0.88 mm was selected as the most efficient design.
- The basic tube obtained the worst rank as expected.

Table 15 The comparison between the selected tube and the basic tube

	f_1 F_i^0	f_2 F_{max}^0	f_3 E^0	f_4 F_i^{15}	f_5 F_{max}^{15}	f_6 E^{15}	f_7 F_i^{30}	f_8 F_{max}^{30}	f_9 E^{30}	f_{10} M
Selected segmented tube	52.8	170.8	8.2	17.6	151.5	7.8	5.6	81.0	5.3	0.36
Basic tube	107.4	107.4	5.8	44.7	84.8	6.3	13.3	55.4	3.8	0.32
Contrast%	50.8	59.0	41.4	60.6	78.7	23.8	57.9	46.2	39.5	12.5

- Although the curve of the basic tube and segmented tube under off-axial loads seemed similar, the maximum load of segmented tube occurred sooner than the basic one.
- According to the ANOVA results, the thickness parameters (t_1 and t_c) play the main role in the models of crashworthiness characters, particularly the thickness of the first segment of the tubes (t_1).
- In sorting different crush scenarios, the typical scenario for investigating the behavior of tube energy absorbers, i.e., under axial loading obtained the seventh rank, which suggests that oblique loading is critical to be considered in optimum design of multi-segmented tubes.

Future work may include performing experiments on the oblique, crush loading of the studied segmented tubes, upon which uncertainty factors may also be brought into the FE

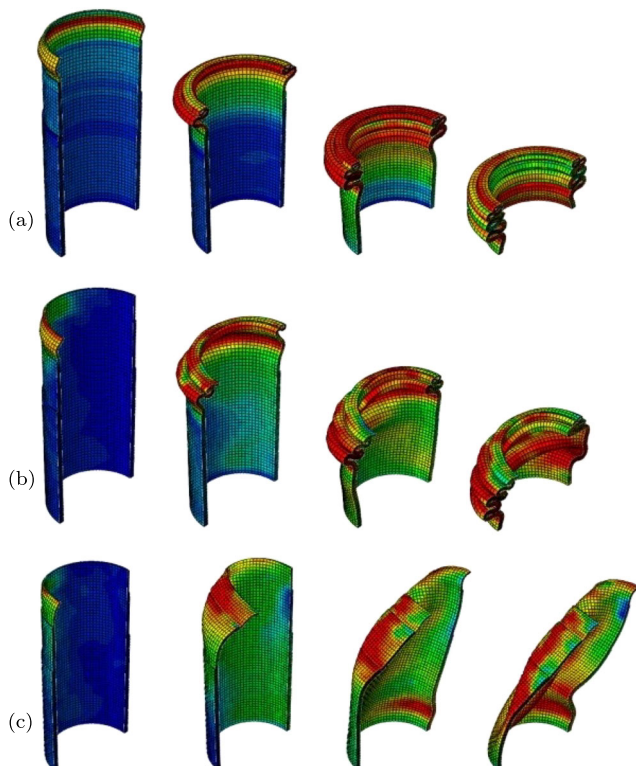


Fig. 14 Deforming process of the selected tube under **a** axial, **b** 15°, and **c** 30° loads

models and perform stochastic optimization of the structure in the virtue of more robust applications in practice.

Compliance with ethical standards

Conflict of interests The authors declare that there is no conflict of interest.

Replication of results For the sake of replication of results and help in using the present study for further research and implementations, the employed materials and methods are provided in the supplementary material of this paper.

References


- Abdi F (2018) Hospital leanness assessment model: a fuzzy multi-moora decision making approach. *J Ind Syst Eng* 11(3):37–59. http://www.jise.ir/article_61899.html
- Adalı EA, Işık AT (2017) The multi-objective decision making methods based on MULTIMOORA and MOOSRA for the laptop selection problem. *J Indust Eng Inter* 13(2):229–237. <https://doi.org/10.1007/s40092-016-0175-5>
- Alavi Nia A, Fallah Nejad K, Badnava H, Farhoudi H (2012) Effects of buckling initiators on mechanical behavior of thin-walled square tubes subjected to oblique loading. *Thin-Walled Struct* 59:87–96. <https://doi.org/10.1016/j.tws.2012.03.002>
- Alemi-Ardakani M, Milani AS, Yannacopoulos S, Shokouhi G (2016) On the effect of subjective, objective and combinative weighting in multiple criteria decision making: a case study on impact optimization of composites. *Expert Syst Appl* 46:426–438. <https://doi.org/10.1016/j.eswa.2015.11.003>
- Alkhatib SE, Tarlochan F, Hashem A, Sassi S (2018) Collapse behavior of thin-walled corrugated tapered tubes under oblique impact. *Thin-Walled Struct* 122(2017):510–528. <https://doi.org/10.1016/j.tws.2017.10.044>
- Baykasoğlu A, Baykasoğlu C (2017) Multiple objective crashworthiness optimization of circular tubes with functionally graded thickness via artificial neural networks and genetic algorithms. *Proc Inst Mech Eng Part C: J Mech Eng Sci* 231(11):2005–2016. <https://doi.org/10.1177/0954406215627181>
- Brauers WKM, Kildiene S, Zavadskas EK, Kaklauskas A (2013) The construction sector in twenty European countries during the recession 2008–2009 – country ranking by MULTIMOORA. *Int J Strateg Prop Manag* 17(1):58–78. <https://doi.org/10.3846/1648715X.2013.775194>
- Brauers WKM, Zavadskas EK (2006) The MOORA method and its application to privatization in a transition economy. *Control Cybern* 35(2):445–469
- Brauers WKM, Zavadskas EK (2010) Project management by MULTIMOORA as an instrument for transition economies. *Technol Econ Dev Econ* 16(1):5–24. <https://doi.org/10.3846/tede.2010.01>

- Brauers WKM, Zavadskas EK (2011) Multimoora optimization used to decide on a bank loan to buy property. *Technol Econ Dev Econ* 17(1):174–188. <https://doi.org/10.3846/13928619.2011.560632>
- Brauers WKM, Zavadskas EK (2012) Robustness of MULTIMOORA : a method for multi-objective optimization. *Informatica* 23(1):1–25
- Čereška A, Podvievko A, Zavadskas E (2018) Assessment of different metal screw joint parameters by using multiple criteria analysis methods. *Metals* 8(5):318. <https://doi.org/10.3390/met8050318>
- Chen S, Yu H, Fang J (2018) A novel multi-cell tubal structure with circular corners for crashworthiness. *Thin-Walled Struct* 122(2017):329–343. <https://doi.org/10.1016/j.tws.2017.10.026>
- Deliktas D, Ustun O (2017) Student selection and assignment methodology based on fuzzy multimoora and multichoice goal programming. *Int Trans Oper Res* 24(5):1173–1195. <https://doi.org/10.1111/itor.12185>
- Ding X, Zhong J (2018) Power battery recycling mode selection using an extended MULTIMOORA method. *Scientific Programming*. <https://doi.org/10.1155/2018/7675094>
- Djameluddin F, Abdullah S, Ariffin A, Nopiah Z (2015) Optimization of foam-filled double circular tubes under axial and oblique impact loading conditions. *Thin-Walled Struct* 87:1–11. <https://doi.org/10.1016/j.tws.2014.10.015>
- Djameluddin F, Abdullah S, Arrifin AK, Nopiah ZM (2018) Crush analysis of the foam-filled bitubal circular tube under oblique impact. *IOP Conference Series: Materials Science and Engineering* 308(1):012040. <https://doi.org/10.1088/1757-899X/308/1/012040>
- Eyvazian A, Tran T, Hamouda AM (2018) Experimental and theoretical studies on axially crushed corrugated metal tubes. *Int J NonLin Mech* 101:86–94. <https://doi.org/10.1016/j.ijnonlinmec.2018.02.009>
- Fattahi R, Khalilzadeh M (2018) Risk evaluation using a novel hybrid method based on FMEA, extended MULTIMOORA, and AHP methods under fuzzy environment. *Saf Sci* 102(2017):290–300. <https://doi.org/10.1016/j.ssci.2017.10.018>
- Firouzi M, Niknejad A, Ziaee S, Hematiyan MR (2018) Optimization of H-shaped thin-walled energy absorber by Taguchi method and a new theoretical estimation for its energy absorption. *Thin-Walled Struct* 131(June):33–44. <https://doi.org/10.1016/j.tws.2018.06.027>
- Gao Q, Wang L, Wang Y, Wang C (2016) Crushing analysis and multiobjective crashworthiness optimization of foam-filled ellipse tubes under oblique impact loading. *Thin Wall Struct* 100:105–112. <https://doi.org/10.1016/j.tws.2015.11.020>
- Ghamarian A, Zarei H (2012) Crashworthiness investigation of conical and cylindrical end-capped tubes under quasi-static crash loading. *Int J Crashworthiness* 17(1):19–28. <https://doi.org/10.1080/13588265.2011.623025>
- Ha NS, Lu G, Xiang X (2018) High energy absorption efficiency of thin-walled conical corrugation tubes mimicking coconut tree configuration. *Int J Mech Sci* 148:409–421. <https://doi.org/10.1016/j.ijmecsci.2018.08.041>
- Hafezalkotob A, Hafezalkotob A (2016) Extended MULTIMOORA method based on Shannon entropy weight for materials selection. *J Ind Eng Int* 12(1):1–13. <https://doi.org/10.1007/s40092-015-0123-9>
- Hafezalkotob A, Hafezalkotob A, Liao H, Herrera F (2018) An overview of MULTIMOORA for multi-criteria decision-making: theory, developments, applications, and challenges. *Information Fusion* <https://doi.org/10.1016/j.inffus.2018.12.002>
- Hafezalkotob A, Hafezalkotob A, Sayadi MK (2016) Extension of multimoora method with interval numbers: an application in materials selection. *Appl Math Model* 40(2):1372–1386
- Hafezalkotob AA, Hafezalkotob AA, Sayadi MK (2016) Extension of MULTIMOORA method with interval numbers: an application in materials selection. *Appl Math Model* 40(2):1372–1386. <https://doi.org/10.1016/j.apm.2015.07.019>
- Ijadi Maghsoodi A, Abouhamzeh G, Khalilzadeh M, Zavadskas EK (2018) Ranking and selecting the best performance appraisal method using the MULTIMOORA approach integrated Shannon's entropy. *Frontiers of Business Research in China* 12(1):2. <https://doi.org/10.1186/s11782-017-0022-6>
- Jafarian N, Rezvani MJ (2019) Crushing behavior of multi-component conical tubes as energy absorber: a comparative analysis between end-capped and non-capped conical tubes. *Eng Struct* 178(2018):128–135. <https://doi.org/10.1016/j.engstruct.2018.09.092>
- Jahan A, Edwards KL, Bahraminasab M (2016) Multi-criteria decision analysis for supporting the selection of engineering materials in product design, 2nd Edn, Butterworth-Heinemann, p 252
- Jahan A, Mustapha F, Sapuan SM, Ismail MY, Bahraminasab M (2012) A framework for weighting of criteria in ranking stage of material selection process. *Int J Adv Manuf Technol* 58(1-4):411–420. <https://doi.org/10.1007/s00170-011-3366-7>
- Jandaghi Shahi V, Marzbanrad J (2012) Analytical and experimental studies on quasi-static axial crush behavior of thin-walled tailor-made aluminum tubes. *Thin Wall Struct* 60:24–37. <https://doi.org/10.1016/j.tws.2012.05.015>
- Kathiresan M, Manisekar K (2016) Axial crush behaviours and energy absorption characteristics of aluminium and E-glass/epoxy over-wrapped aluminium conical frusta under low velocity impact loading. *Compos Struct* 136(1):86–100. <https://doi.org/10.1016/j.compstruct.2015.09.052>
- Khalkhali A, Mostafapour M, Tabatabaie SM, Ansari B (2016) Multi-objective crashworthiness optimization of perforated square tubes using modified NSGAII and MOPSO. *Struct Multidiscip Optim* 54(1):45–61. <https://doi.org/10.1007/s00158-015-1385-y>
- Kovach J, Cho BR (2009) A D-optimal design approach to constrained multiresponse robust design with prioritized mean and variance considerations. *Comput Ind Eng* 57(1):237–245. <https://doi.org/10.1016/j.cie.2008.11.011>
- Liang W, Zhao G, Hong C (2018) Selecting the optimal mining method with extended multi-objective optimization by ratio analysis plus the full multiplicative form (MULTIMOORA) approach. *Neural Comput Applic* 5(2):1–16. <https://doi.org/10.1007/s00521-018-3405-5>
- Liu H-C, Zhao H, You X-Y, Zhou W-Y (2019) Robot evaluation and selection using the hesitant fuzzy linguistic MULTIMOORA method. *J Test Eval* 47(2):20170094. <https://doi.org/10.1520/JTE20170094>
- Lu G, Yu TX (2003) Energy absorption of structures and materials. woodhead publishing limited. <https://doi.org/10.1533/9781855738584>
- Maghsoodi AI, Mosavatb M, Hafezalkotob A, Hafezalkotob A (2018) Hybrid hierarchical fuzzy group decision-making based on information axioms and BWM. *Prototype design selection*. *Computers &, Industrial Engineering*, pp 1–17. <https://doi.org/10.1016/j.cie.2018.11.018>
- Montgomery DC (2017) Design and analysis of experiments. John Wiley & Sons
- Nahas M (1993) Impact energy dissipation characteristics of thin-walled cylinders. *Thin-walled Structures* 15(2):81–93
- Niknejad A, Abedia MM, Liaghatb GH, Zamani Nejada M (2015) Absorbed energy by foam-filled quadrangle tubes during the crushing process by considering the interaction effects. *Archives of Civil and Mechanical Engineering* 15(2):376–391. <https://doi.org/10.1016/j.acme.2014.09.005>
- Pirmohammad S, Esmaeili-Marzdashti S, Eyvazian A (2019) Crashworthiness design of multi-cell tapered tubes using response surface methodology. *J Comput Appl Res Mech Eng (JCARME)* 9(1):59–75. <https://doi.org/10.22061/jcarme.2018.2825.1292>

- Qi C, Yang S, Dong F (2012) Crushing analysis and multiobjective crashworthiness optimization of tapered square tubes under oblique impact loading. *Thin Wall Struct* 59:103–119. <https://doi.org/10.1016/j.tws.2012.05.008>
- Ravi Sankar H, Parameswaran V (2018) Effect of circular perforations on the progressive collapse of circular cylinders under axial impact. *Int J Impact Eng* 122:346–362. <https://doi.org/10.1016/j.ijimpeng.2018.09.001>
- Reyes A, Langseth M, Hopperstad O (2003) Square aluminum tubes subjected to oblique loading. *Int J Impact Eng* 28(10):1077–1106. [https://doi.org/10.1016/S0734-743X\(03\)00045-9](https://doi.org/10.1016/S0734-743X(03)00045-9)
- Rezvani MJ (2017) Experimental and numerical simulation investigation on crushing response of foam-filled conical tubes stiffened with annular rings. *J Solid Mech* 9(2):291–301
- Saeidi Googarchin H, Pasandidehpoor M, Mahmoodi A, Shojaeefard M (2018) Energy absorption analysis for tapered multi-cell tubes improved by foams: theoretical development and numerical simulation. *Compos Struct* 207(2018):213–222. <https://doi.org/10.1016/j.compstruct.2018.09.032>
- Song X, Sun G, Li G, Gao W, Li Q (2013) Crashworthiness optimization of foam-filled tapered thin-walled structure using multiple surrogate models. *Struct Multidiscip Optim* 47(2):221–231
- Souzangarzadeh H, Rezvani MJ, Jahan A (2017) Selection of optimum design for conical segmented aluminum tubes as energy absorbers: application of MULTIMOORA method. *Appl Math Model* 51:546–560. <https://doi.org/10.1016/j.apm.2017.07.005>
- Stanujkic D, Zavadskas EK, Brauers WKM, Karabasevic D (2015) An extension of the multimooora method for solving complex decision-making problems based on the use of interval-valued triangular fuzzy numbers. *Transformations in Business & Economics* 14(2B):355–375
- Stanujkic D, Zavadskas EK, Smarandache F, Brauers WK, Karabasevic D (2017) A neutrosophic extension of the MULTIMOORA method. *Informatica* 28(1):181–192. <https://doi.org/10.15388/Informatica.2017.125>
- Sun G, Liu T, Fang J, Steven GP, Li Q (2018) Configurational optimization of multi-cell topologies for multiple oblique loads. *Struct Multidiscip Optim* 57(2):469–488. <https://doi.org/10.1007/s00158-017-1839-5>
- Supian A, Sapuan S, Zuhri M, Zainudin E, Ya H (2018) Hybrid reinforced thermoset polymer composite in energy absorption tube application: a review. *Def Technol* 14(4):291–305. <https://doi.org/10.1016/j.dt.2018.04.004>
- Taştan A, Acar E, Güler M, Kılınçkaya Ü (2016) Optimum crashworthiness design of tapered thin-walled tubes with lateral circular cutouts. *Thin-Walled Structures* 107. <https://doi.org/10.1016/j.tws.2016.07.018>
- Tasdemirci A, Sahin S, Kara A, Turan K (2015) Crushing and energy absorption characteristics of combined geometry shells at quasi-static and dynamic strain rates: experimental and numerical study. *Thin-Walled Struct* 86:83–93
- Tran T, Baroutaji A (2018) Crashworthiness optimal design of multi-cell triangular tubes under axial and oblique impact loading. *Eng Fail Anal* 93:241–256. <https://doi.org/10.1016/j.engfailanal.2018.07.003>
- Wang D-Z, Cao G-J, Qi C, Sun Y, Yang S, Du Y (2016) Crushing analysis and lightweight design of tapered tailor welded hybrid material tubes under oblique impact. *SAE Int J Mater Manuf* 9(3):2016–01–0407. <https://doi.org/10.4271/2016-01-0407>
- Wu F, Xiao X, Yang J, Gao X (2018) Quasi-static axial crushing behaviour and energy absorption of novel metal rope crochetsintered mesh tubes. *Thin-Walled Struct* 127(February):120–134. <https://doi.org/10.1016/j.tws.2018.02.004>
- Yang S, Qi C (2013) Multiobjective optimization for empty and foam-filled square columns under oblique impact loading. *Int J Impact Eng* 54:177–191. <https://doi.org/10.1016/j.ijimpeng.2012.11.009>
- Ying L, Dai M, Zhang S, Ma H, Hu P (2017) Multiobjective crashworthiness optimization of thin-walled structures with functionally graded strength under oblique impact loading. *Thin Wall Struct* 117:165–177. <https://doi.org/10.1016/j.tws.2017.04.007>
- Zahran M, Xue P, Esa M, Abdelwahab M (2018) A novel tailor-made technique for enhancing the crashworthiness by multi-stage tubular square tubes. *Thin-Walled Struct* 122(2017):64–82. <https://doi.org/10.1016/j.tws.2017.09.031>
- Zavadskas EK, Antucheviciene J, Razavi Hajiagha SH, Hashemi SS (2015) The interval-valued intuitionistic fuzzy multimooora method for group decision making in engineering. *Math Probl Eng* 2015(2):560690, (13 pp.) <https://doi.org/10.1155/2015/560690>
- Zavadskas EK, Bausys R, Juodagalviene B, Garnyte-Sapranaviciene I (2017) Model for residential house element and material selection by neutrosophic MULTIMOORA method. *Eng Appl Artif Intell* 64(May):315–324. <https://doi.org/10.1016/j.engappai.2017.06.020>
- Zhang H, Zhang X (2016) Crashworthiness performance of conical tubes with nonlinear thickness distribution. *Thin-Walled Struct* 99:35–44. <https://doi.org/10.1016/j.tws.2015.11.007>
- Zhang L, Bai Z, Bai F (2018) Crashworthiness design for bio-inspired multi-cell tubes with quadrilateral, hexagonal and octagonal sections. *Thin-Walled Struct* 122(2017):42–51. <https://doi.org/10.1016/j.tws.2017.10.010>
- Zhang Y, Sun G, Xu X, Li G, Li Q (2014) Multiobjective crashworthiness optimization of hollow and conical tubes for multiple load cases. *Thin-Walled Struct* 82:331–342. <https://doi.org/10.1016/j.tws.2014.05.006>
- Zhao H, You J-X, Liu H-C (2016) Failure mode and effect analysis using multimooora method with continuous weighted entropy under interval-valued intuitionistic fuzzy environment. *Soft Computing*. <https://doi.org/10.1007/s00500-016-2118-x> (in press)

Publisher's note Springer Nature remains neutral with regard to jurisdictional claims in published maps and institutional affiliations.

Affiliations

Hamidreza Souzangarzadeh¹  · Ali Jahan² · Mohammad Javad Rezvani¹ · Abbas S. Milani³

Ali Jahan
iranaliarahan@yahoo.com

Mohammad Javad Rezvani
rezvani57@gmail.com

Abbas S. Milani
abbas.milani@ubc.ca

- ¹ Department of Mechanical Engineering, Semnan Branch, Islamic Azad University, Semnan, Iran
- ² Department of Industrial Engineering, Semnan Branch, Islamic Azad University, Semnan, Iran
- ³ School of Engineering, University of British Columbia, Kelowna, BC V1V 1V7, Canada